ELSEVIER

PII: S0032-3861(97)00457-6

Polymer Vol. 39 Nos. 8–9, pp. 1727–1734, 1998

0032-3861/97/$17.00+0.00

The effect of glass transition temperature on the crystallization of ε-caprolactone–styrene diblock copolymers

Shuichi Nojima*, Hiroyuki Tanaka, Awaludin Rohadi and Shintaro Sasaki
School of Materials Science, Japan Advanced Institute of Science and Technology (JAIST), Tatsunokuchi, Ishikawa, 923-12, Japan
(Received 8 April 1997; revised 14 May 1997)

The morphology and melting behaviour of ε-caprolactone–styrene diblock copolymers (PCL-*b*-PS) quenched from the melt were investigated by small-angle X-ray scattering and differential scanning calorimetry as a function of glass transition temperature of the PS block, $T_{g,PS}$. A plasticizer miscible only with the PS block, such as polystyrene oligomer or dioctyl phthalate, was added to PCL-*b*-PS in order to decrease $T_{g,PS}$ successively (plasticizer-added PCL-*b*-PS). The crystallizability of the PCL block depended strongly on $T_{g,PS}$; the PCL block did not crystallize when $T_{g,PS}$ was higher than the crystallization temperature T_c, while it crystallized partially when $T_{g,PS}$ was lower than T_c. However, details of the morphology formed (i.e. the long spacing and lamellar thickness) were independent of $T_{g,PS}$. These results suggest that the mobility of PCL-*b*-PS influences extremely the crystallizability of the PCL block, but not the resulting morphology. The morphologies formed in the plasticizer-added PCL-*b*-PS were compared with those of PCL-*b*-PS cast from toluene or cyclohexane solution, and the characteristics of these morphologies were qualitatively discussed.

(Keywords: crystalline–amorphous diblock copolymer; glass transition temperature; crystallization)

INTRODUCTION

Crystalline–amorphous diblock copolymers are a fascinating system for studying the cooperative morphology formation in polymer systems. In these copolymers, the crystallization starts from the microdomain structure when they are quenched from the melt. The molecular characteristics of the constituent block copolymer, such as total molecular weight, block ratio, interaction between the blocks, and glass transition temperature (T_g) of the amorphous block, all affect the subsequent crystallization behaviour and eventually the final morphology. In a high molecular weight copolymer, for example, the crystallization takes place within the microdomain structure existing at the melt to yield the immature crystallites[1–6]. In a low molecular weight copolymer, on the other hand, a morphological reorganization is observed from a microdomain structure into a lamellar morphology, an alternating structure of crystalline lamellae and amorphous layers[7–16]. This difference in the crystallization behaviour arises mainly from the stability of the microdomain structure; when the molecular weight is not large, the microdomain structure is in a weak segregation to be easily destroyed by the following crystallization, while the molecular weight is large enough, it is in a strong segregation to yield a high energy barrier for the destruction of this structure.

When the T_g of the amorphous block is close to the crystallization temperature (T_c) or higher than T_c, an additional complexity intervenes in the morphology formation. That is, the restricted mobility of the block copolymer yields a significant effect on the subsequent crystallization. There are some studies on the morphology of crystalline–amorphous diblock copolymers with a high T_g amorphous block[17–22]. Liu and coworkers[21,22], for example, investigated the morphology and morphology formation of tetrahydrofuran–methyl methacrylate diblock copolymers (PTHF-*b*-PMMA), where the T_g of the PMMA block was *ca* 105°C and the melting temperature (T_m) of the PTHF block was *ca* 30°C, and showed that the crystallization behaviour of the solution-cast PTHF-*b*-PMMA was strongly dependent on the molecular characteristics and crystallization conditions.

In this study, we investigate the morphology and melting behaviour of various ε-caprolactone–styrene diblock copolymers (PCL-*b*-PS), where the T_g of the PS block, $T_{g,PS}$, is *ca* 95°C and the T_m of the PCL block is *ca* 50°C. It is expected that the PS block has completely frozen before the PCL block starts to crystallize when PCL-*b*-PS is quenched from the melt. It is, therefore, necessary to decrease $T_{g,PS}$ and eventually to increase the crystallizability of the PCL block by blending a plasticizer (plasticizer-added PCL-*b*-PS). The melting temperature and crystallinity of the PCL block were measured by differential scanning calorimetry (d.s.c.) and the resulting morphology was also investigated by small-angle X-ray scattering (SAXS). The morphology formed in the plasticizer-added PCL-*b*-PS was compared with that of PCL-*b*-PS cast from toluene or cyclohexane solution, and we discuss qualitatively the morphology formation of the present PCL-*b*-PS/plasticizer systems.

EXPERIMENTAL

Materials

The PCL-*b*-PS copolymers used in this study were synthesized by successive anionic polymerizations under

* To whom correspondence should be addressed

Table 1 Characterization of polymers

Notation	Polymer	Source	Total M_n^a	M_w/M_n^b	PCL/PS ratio (vol%)[c]
A1	PCL-*b*-PS	[d]	12000	1.41	34/66
A2	PCL-*b*-PS	[d]	23000	1.21	26/74
A3	PCL-*b*-PS	[d]	12000	1.18	13/87
PS1	PSO	[e]	500	1.14	—
PS2	PSO	[e]	950	1.13	—

[a] Determined by VPO [b] Determined by g.p.c. [c] Determined by ^{1}H n.m.r. [d] Synthesized in our laboratory [e] Obtained from TOSOH Corporation

vacuum. The styrene monomer was first polymerized in toluene at 20°C for 24 h with *n*-butyllithium as an initiator, then ε-caprolactone monomer was added to synthesize the block copolymer at − 15°C over 2~12 min. The reaction time of the ε-caprolactone monomer was carefully adjusted to obtain the PCL block with various molecular weights and also to prevent depolymerization (backbiting) by the living ε-caprolactone end during the anionic growth of the PCL block[23]. The block copolymers were precipitated several times into methanol to remove the unreacted ε-caprolactone monomer.

The samples thus synthesized were characterized by gel permeation chromatography (g.p.c.), vapour pressure osmometry (VPO), and nuclear magnetic resonance (^{1}H n.m.r). *Table 1* summarizes the results of molecular characterization. The following specific volumes were used to calculate the block ratio in vol% from the ^{1}H n.m.r. result and the electron density of each block for the SAXS measurement. For polystyrene[24] (above T_g),

$$v_{sp} = 0.9217 + (5.412 \times 10^{-4}) \times T + (1.687 \times 10^{-7}) \times T^2 \quad (1)$$

and for amorphous poly(ε-caprolactone)[25],

$$v_{sp} = 0.9106 + (6.013 \times 10^{-4}) \times T \quad (2)$$

where v_{sp} is in $cm^3\ g^{-1}$ and T is in °C. For the perfect crystal of poly(ε-caprolactone)[26], $v_{sp} = 0.833\ cm^3\ g^{-1}$ was used irrespective of temperature.

Sample preparation

Two methods were employed to promote the crystallization of the PCL block in PCL-*b*-PS. In the first method, polystyrene oligomer (PSO) or dioctyl phthalate (DOP), miscible only with the PS block, was blended with PCL-*b*-PS (plasticizer-added PCL-*b*-PS) in order to decrease $T_{g,PS}$ and eventually enhance the crystallizability of the PCL block. In the other method, the PCL-*b*-PS solution was cast on a glass plate at T_c to give the opportunity for the PCL block to crystallize during the gradual evaporation of the solvent (solution-cast PCL-*b*-PS).

The molecular characteristics of PSO used for the plasticizer-added PCL-*b*-PS are shown in *Table 1*. PSO is known to be immiscible with PCL homopolymer[27,28] and DOP was also immiscible with PCL, so that they are accommodated selectively into the PS block domain at the melt to decrease $T_{g,PS}$. PCL-*b*-PS and plasticizer were first dissolved in a common solvent benzene and the solvent was evaporated at 100°C for more than 24 hr under vacuum. The sample was then quenched to T_c ranging from 20°C to 40°C and annealed at T_c for 24 hr to crystallize the PCL block.

To prepare the solution-cast PCL-*b*-PS, two solvents were used; toluene, good for both blocks at any temperatures, and cyclohexane, good for both blocks above 35°C and poor only for the PCL block below 35°C. The solution was cast on a glass plate and the solvent was evaporated gradually at T_c ranging from 20 to 50°C for more than 24 h, during which the PCL block crystallized.

Small-angle X-ray scattering measurements

The SAXS measurement was performed with a point focusing optics and a one-dimensional position sensitive proportional counter (PSPC) with an effective length of 10 cm. The accumulation time for each measurement was 3000~5000 s. Details of the optics and the instrumentation are described elsewhere[29,30]. The SAXS intensity measured was corrected for the background scattering and absorption by the sample, and relative scattered intensity $I(s)$ was obtained as a function of wave number s defined by

$$s = 2\sin\theta/\lambda \quad (3)$$

where 2θ is the scattering angle and λ is the X-ray wave length (= 0.1542 nm). Since the apparatus had point focusing optics, the scattered intensity was not corrected for the smearing effect from the finite cross section of the primary beam. The angular position of the intensity peak was evaluated after the SAXS curve was corrected for the Lorentz factor.

The electron density difference between the amorphous PCL (337 e nm^{-3} at 100°C) and PS (332 e nm^{-3} at 100°C) is unfortunately extremely small, so that we can not expect the scattering from the microdomain structure at the melt. It is also impossible to observe the change of the microdomain structure by adding the plasticizer. The scattering from the morphology after crystallization of the PCL block, however, can be observed since there is an enough electron density difference between PCL crystals (393 e nm^{-3}) and PS blocks (344 e nm^{-3} at 40°C).

Differential scanning calorimetry measurements

A Perkin-Elmer Model 7 DSC was used to determine $T_{g,PS}$, melting temperature of the PCL block $T_{m,PCL}$, and crystallinity of the PCL block χ (i.e. wt% of the crystallized PCL blocks against the existing PCL blocks in the system). The plasticizer-added and solution-cast samples in which the PCL block crystallized were heated at a rate of 5°C min^{-1}. $T_{g,PS}$ was evaluated from the onset of the baseline change, $T_{m,PCL}$ was evaluated from the endothermic peak position, and χ was calculated from the peak area assuming that the heat of fusion for the perfect PCL crystal is 135.44 J g^{-1} [23]. When $T_{g,PS}$ and $T_{m,PCL}$ were overlapped in a same temperature range, $T_{g,PS}$ was evaluated using the samples just quenched from the melt, where the PCL block did not start to crystallize.

RESULTS

Crystallization of plasticizer-added PCL-b-PS

The PCL-*b*-PS copolymers synthesized in this study did not crystallize when they were quenched from the melt into

any crystallization temperatures ranging from 0°C to $T_{m,PCL}$. This fact was confirmed by the d.s.c. curve with no endothermic peak for the melting and also by the monotonously decreasing SAXS curve with increasing s. This result is intuitively understood from the fact that the T_g of the amorphous block (PS block) is higher than the T_m of the crystallizable block (PCL block) and hence PCL-*b*-PS can not move favourably for the crystallization at T_c.

Differential scanning calorimetry measurements. The crystallization of the PCL block was induced by adding PSO with $M_n = 500$ (PS1) or 950 (PS2) (*Table 1*) or DOP selectively to the PS block and eventually by decreasing $T_{g,PS}$. The d.s.c. thermograms for A2/PS1 crystallized at T_c = 30°C for 24 h are shown in *Figure 1*, where each curve is adjusted so as to show the result for the unit gram of the PCL block and ϕ_{PS} represents the weight fraction of the PS block against the sum of the PS block and plasticizer in the system. The endothermic area increases with decreasing ϕ_{PS}, namely, with increasing the plasticizer in the system. The ϕ_{PS} dependence of $T_{g,PS}$ and $T_{m,PCL}$ for A2/PS1, A2/PS2, and A2/DOP is shown in *Figure 2*. In *Figure 2*a, $T_{g,PS}$ decreases linearly with decreasing ϕ_{PS}, indicating that $T_{g,PS}$ is simply described by a linear combination of the T_gs of the components:

$$T_{g,PS} = (1 - \phi_{PS})T_{g,1} + \phi_{PS}T_{g,2} \quad (4)$$

where $T_{g,1}$ and $T_{g,2}$ represent the T_gs of the plasticizer used and the pure PS block (~95°C), respectively. The single and ϕ_{PS} dependent $T_{g,PS}$ shown in *Figure 2*a means that the plasticizer is completely miscible with the PS block in the microdomain structure at the melt, and also that it is possible

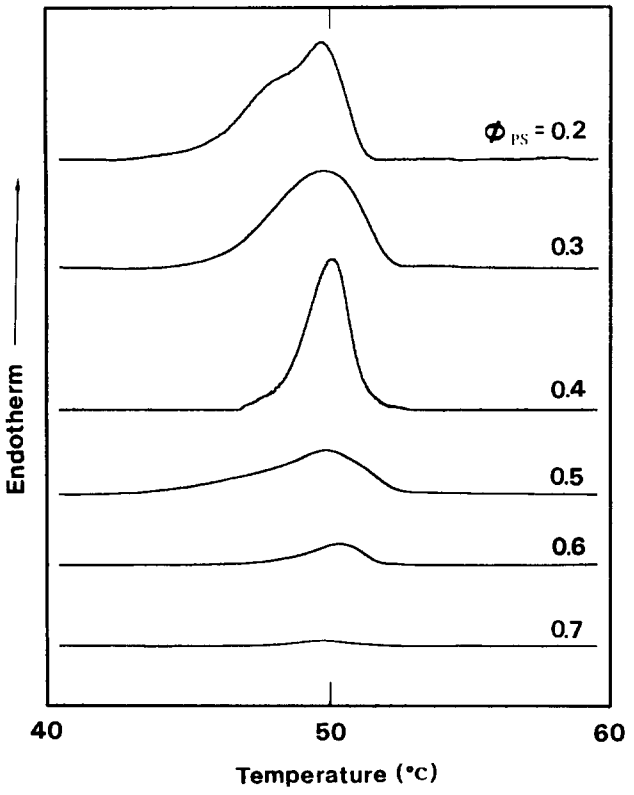

Figure 1 D.s.c. thermograms for A2/PS1 systems crystallized at 30°C for 24 h. The heating rate is 5°C min^{-1}. ϕ_{PS} represents the weight fraction of the PS block against the sum of the PS block and added plasticizer. The d.s.c. curves are adjusted so as to show the result for the unit gram of the PCL block

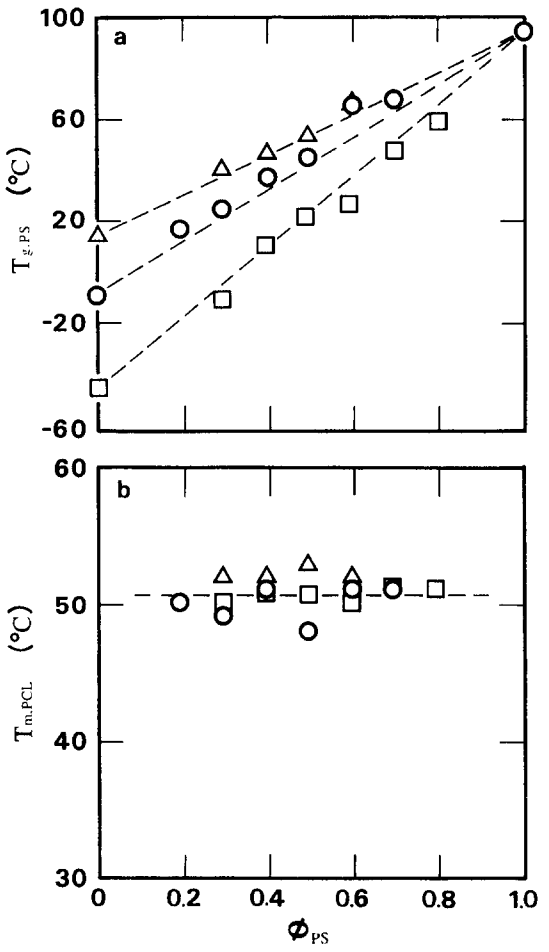

Figure 2 ϕ_{PS} dependence of $T_{g,PS}$ (a) and $T_{m,PCL}$ (b) for A2/PS1 (○), A2/PS2 (△), and A2/DOP (□). T_c = 30°C

to change the mobility of PCL-*b*-PS arbitrarily by changing ϕ_{PS} when trying to crystallize the PCL block at T_c. The addition of a large amount of the plasticizer will produce a considerable deformation of the microdomain structure, or it may bring the system into a different structure, but we can extract no information about this structure from the d.s.c. results as well as the SAXS results. Though the influence of this structure on the subsequent crystallization is also an interesting topic, we focus on the T_g dependence of the crystallization in this study.

The value of $T_{m,PCL}$ in *Figure 2*b is, on the other hand, almost constant (~50°C) irrespective of ϕ_{PS} and slightly lower than the T_m of PCL homopolymers (~55°C). The melting temperature T_m of crystalline homopolymers is related to the lamellar thickness ℓ_c through the equation[31]

$$T_m = T_m^\circ\{1 - 2\sigma/(\ell_c \Delta H)\} \quad (5)$$

where T_m° is the T_m of the infinitely large crystal, σ is the specific surface energy, and ΔH is the heat of fusion per unit volume. Therefore the constant $T_{m,PCL}$ shown in *Figure 2*b means that ℓ_c is unchanged irrespective of ϕ_{PS}. This is surprising because the difference in ϕ_{PS} leads to the difference in the mobility of PCL-*b*-PS (*Figure 2*a) and eventually to the large difference in crystallinity of the PCL block, but no difference in the characteristics of the resulting morphology (such as the lamellar thickness and long spacing), as described later.

The ϕ_{PS} dependence of $T_{g,PS}$ and $T_{m,PCL}$ for A1/PS1, A2/PS1, and A3/PS1 is shown in *Figure 3*, where samples were

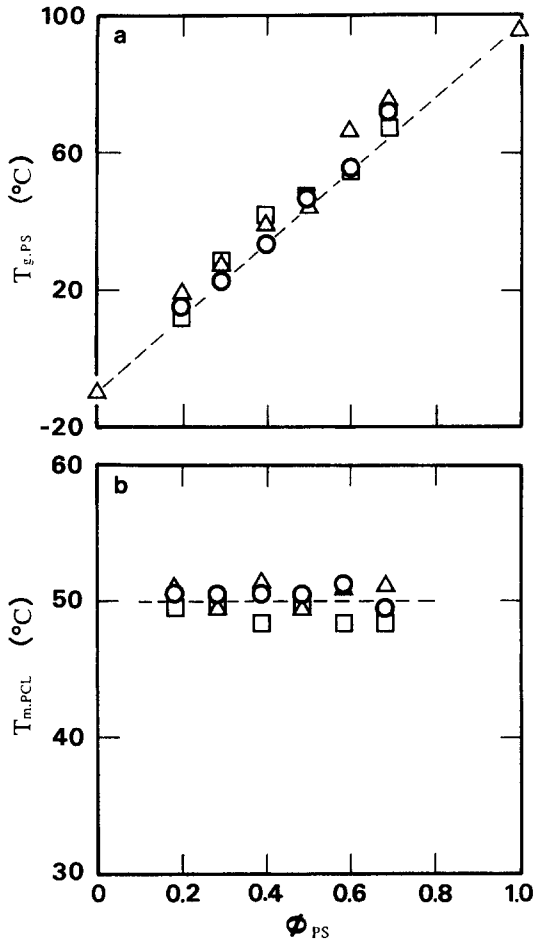

Figure 3 ϕ_{PS} dependence of $T_{g,PS}$ (a) and $T_{m,PCL}$ (b) for A1/PS1 (○), A2/PS1 (□), and A3/PS1 (△). $T_c = 30$°C

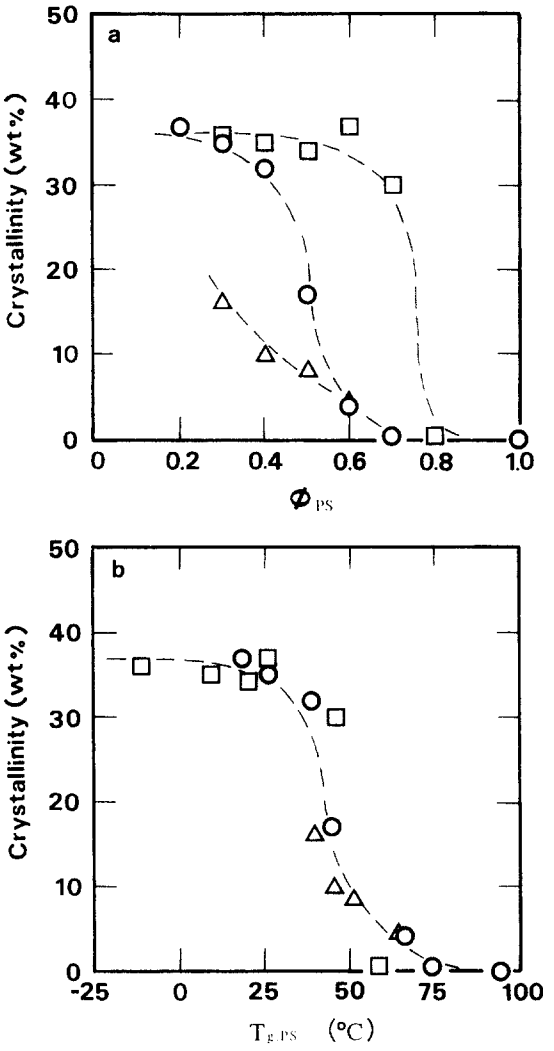

Figure 4 (a) ϕ_{PS} dependence of χ and (b) $T_{g,PS}$ dependence of χ for A2/PS1 (○), A2/PS2 (△), and A2/DOP (□). $T_c = 30$°C

crystallized at 30°C for 24 h for the $T_{m,PCL}$ measurement. $T_{g,PS}$ falls on a single straight line connecting the T_gs of the PS block and PS1, suggesting that the ϕ_{PS} dependence of $T_{g,PS}$ is not affected by the molecular weight of the constituent PS block, since the PS block is enough long for each PCL-*b*-PS. The value of $T_{m,PCL}$ is *ca* 50°C and independent of ϕ_{PS}. We could not observe the difference in $T_{g,PS}$ and $T_{m,PCL}$ measured by d.s.c. among A1, A2, and A3, so we describe mainly the results of A2/plasticizer systems hereafter.

The crystallinity of the PCL block, χ, is plotted against ϕ_{PS} in *Figure 4*a, where each system makes different curves which change suddenly within a narrow ϕ_{PS} range. In A2/DOP, for example, ϕ changes dramatically in the ϕ_{PS} range 0.7~0.8. It is possible to convert ϕ_{PS} into $T_{g,PS}$ of each system by using equation (4) obtained in *Figure 2*a. The plot of χ against $T_{g,PS}$ for three systems is shown in *Figure 4*b. The three different curves in *Figure 4*a coincide with each other and make one master curve in *Figure 4*b. The temperature at which χ changes dramatically is about 40°C, which is slightly higher than T_c (= 30°C). *Figure 4* suggests that the crystallizability of the PCL block is extremely affected by $T_{g,PS}$, and that when PCL-*b*-PS has an enough mobility at T_c, the PCL block crystallizes.

When T_c was changed between 20 and 40°C, the χ *versus* ϕ_{PS} curve (*Figure 4*a) and the χ *versus* $T_{g,PS}$ curve (*Figure 4* b) shifted slightly with changing T_c. These curves coincided practically with each other when the abscissa was replaced by $T_c - T_{g,PS}$ instead of $T_{g,PS}$. This indicates that χ is determined by the mobility of PCL-*b*-PS at T_c which relates intimately how far T_c is apart from $T_{g,PS}$ and that $T_c - T_{g,PS}$ is a measure for χ in the present systems.

Small angle X-ray scattering measurements. The Lorentz-corrected SAXS curves for A2/PS1 crystallized at 30°C for 24 h are shown in *Figure 5*, where the SAXS intensity is very weak and we can observe the scattering of the data points at high angles. The SAXS intensity for the samples including A3 or PS2 was also very weak and we could not observe the significant change in the SAXS curve with changing ϕ_{PS}. This is because the scattered intensity is proportional to $\psi(1-\psi)$, where ψ is the volume fraction of the PCL crystal formed in the system, and the A3/plasticizer systems have a low PCL content (*Table 1*) and the PCL-*b*-PS/PS2 systems have a low crystallinity (*Figure 4*a) both leading to a small ψ. *Figure 5* shows that the SAXS curve for $\phi_{PS} = 0.7$ or higher is a monotonously decreasing curve with increasing s, suggesting that there is no regular structure detectable by the SAXS measurement. The SAXS curves for $\phi_{PS} \leq 0.5$, on the other hand, have an intensity peak at around s~0.025 nm^{-1} and also a second intensity peak (indicated by arrows), the position of which exactly corresponds to twice the angular position of the first peak. The appearance of the SAXS intensity peak at $\phi_{PS} \leq 0.5$, which agrees with the finite χ in *Figure 4*, suggests that the

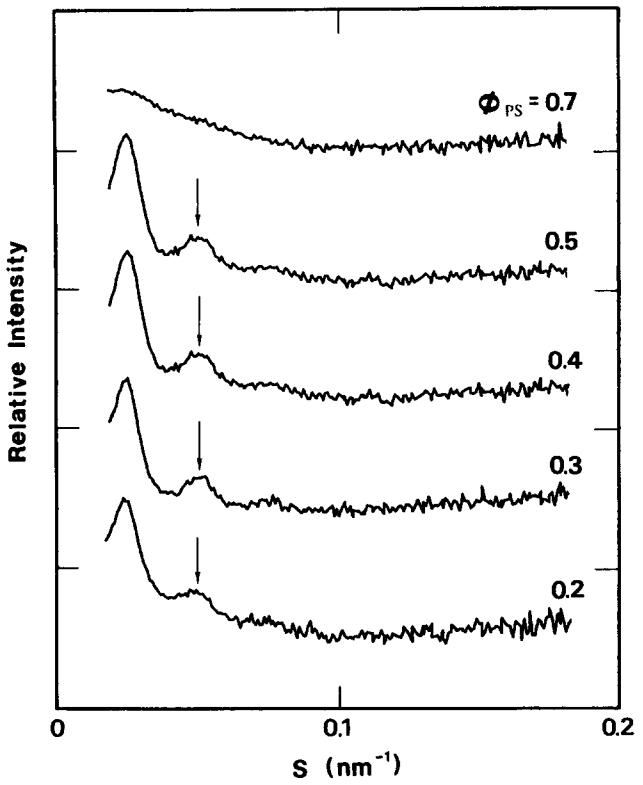

Figure 5 Lorentz-corrected SAXS curves for A2/PS1 crystallized at 30°C for 24 h. The SAXS curves for ϕ_{PS} = 0.3, 0.4, 0.5, and 0.7 are shifted upward successively for legibility

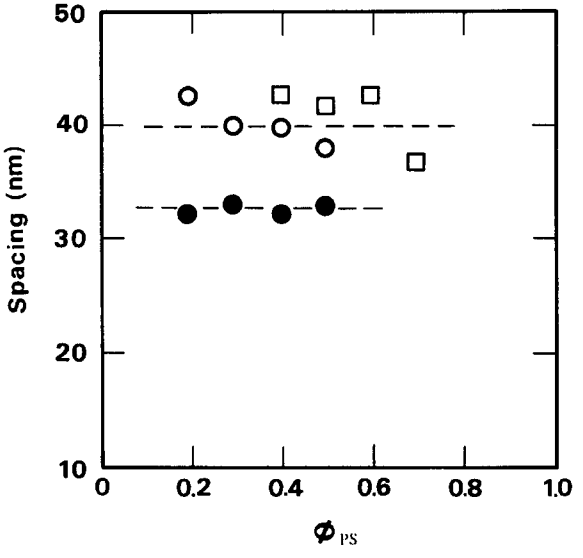

Figure 6 ϕ_{PS} dependence of the long spacing for A2/PS1 (○), A2/DOP (□), and A1/PS1 (●) crystallized at 30°C for 24 h

morphology with a regularly repeating structure is formed by the crystallization of the PCL block. The angular position of the first and second peaks gives a clue to understanding the resulting morphology, as discussed later.

Figure 6 shows the long spacing, L, evaluated from the angular position of the SAXS intensity peak, where L does not change significantly with changing ϕ_{PS} (or mobility of PCL-*b*-PS). However, L increased with increasing T_c and it was also dependent on the copolymer (A1, A2, or A3) used but not the plasticizer (PS1, PS2, or DOP). These facts, together with the constant $T_{m,PCL}$ against ϕ_{PS}, indicate that the mobility of PCL-*b*-PS does not control the details of the morphology (i.e. the long spacing and lamellar thickness) formed by the crystallization in the present systems.

The d.s.c. and SAXS results have revealed that the mobility of PCL-*b*-PS is an important factor for the crystallization of the PCL block. This means that when PCL-*b*-PS has an enough mobility at T_c, then the PCL block can crystallize and χ increases. However, the characteristics of the morphology, such as the long spacing and lamellar thickness, are not determined by the mobility of PCL-*b*-PS, but may be predominantly controlled by T_c. These facts are reminiscent of our previous observations in ϵ-caprolactone-butadiene diblock copolymers (PCL-*b*-PB)[8,11,15], where the T_g of the PB block, $T_{g,PB}$, was extremely low (i.e. $T_c - T_{g,PB} \gg 0$). The PCL block, therefore, crystallized easily by destroying the microdomain structure, and the long spacing of the resulting morphology was strongly dependent on T_c.

Morphological comparison between plasticizer-added PCL-b-PS and solution-cast PCL-b-PS

The other way to provide the mobility to PCL-*b*-PS during crystallization is the solution-casting method; it gives the opportunity for the PCL block to crystallize during the solvent evaporation since PCL-*b*-PS in the solution has an enough mobility. We used two casting solvents: toluene, good for both blocks at any temperatures; and cyclohexane, good for both blocks above 35°C but poor only for the PCL block below 35°C. This means that in the cyclohexane solution below 35°C, $T_{g,PS}$ is extremely low and the crystallization of the PCL block is not disturbed since only the PS block is swollen by cyclohexane.

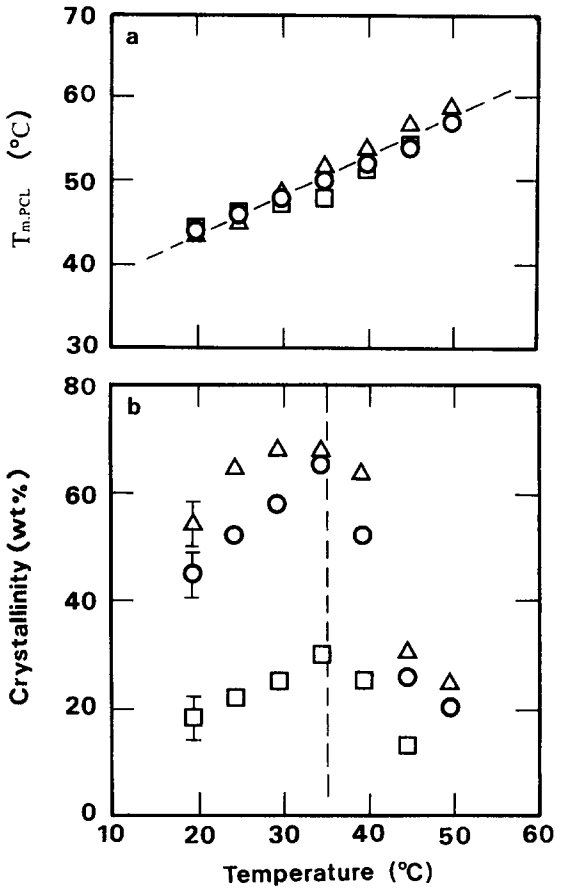

Figure 7 T_c dependence of $T_{m,PCL}$ (a) and χ (b) for A1 (○), A2 (△), and A3 (□) cast from the cyclohexane solution

Differential scanning calorimetry measurements. $T_{m,PCL}$ and χ for A1, A2, and A3 cast from the cyclohexane solution are plotted against T_c in *Figure 7*, where $T_{m,PCL}$ increases linearly with increasing T_c irrespective of the PCL-*b*-PS used. This T_c dependence of $T_{m,PCL}$ was also observed for A2 cast from the toluene solution, and usually observed in the homopolymer crystallization; the increase of T_m is explained by the increase of the lamellar thickness through equation (5). The value of χ was strongly dependent on the solvent used; when toluene was used, χ was low (~20 wt%) and independent of T_c, while χ showed a complicated change with changing T_c when cyclohexane was used, as shown in *Figure 7*b. In *Figure 7*b, χ increases first with increasing T_c and then decreases with further increase of T_c. All three curves begin to decrease when T_c reaches 35°C, where the PCL block starts to be swollen by cyclohexane in the solution. That is, only the PS block is swollen by cyclohexane below 35°C to increase the mobility of PCL-*b*-PS leading to the crystallization of the PCL block, while above 35°C, both PS and PCL blocks are swollen to increase the mobility of PCL-*b*-PS and simultaneously to make the crystallization of the PCL block disturbed. This situation is the same when toluene is used as the casting solvent, where both blocks are swollen by toluene at any temperatures. The value of χ at the same T_c changes significantly for three samples, which is different from the case of the plasticizer-added PCL-*b*-PS (*Figure 4*b).

Small angle X-ray scattering measurements. The SAXS curves for A1 and A2 cast from the cyclohexane solution at each T_c have an intensity peak arising from the lamellar morphology, though the height of the peak changes significantly with changing T_c. The long spacing, L', evaluated from the angular position of the SAXS peak is shown in *Figure 8*, where L' increases slightly with increasing T_c. It is found that L' (*Figure 8*) is significantly smaller than L (*Figure 6*) for the same PCL-*b*-PS crystallized at 30°C, that is, L~40 nm and L'~30 nm for A2 and L~32 nm and L'~25 nm for A1. To understand the morphological difference between the plasticizer-added PCL-*b*-PS and solution-cast PCL-*b*-PS, it is necessary to clarify the general picture of the morphology after crystallization of the PCL block, as discussed later.

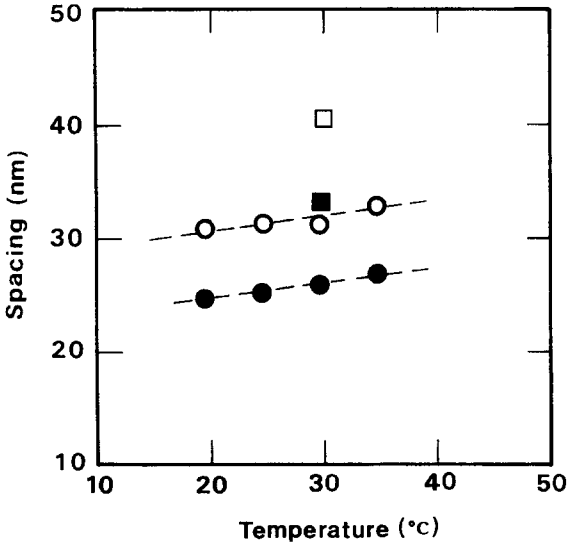

Figure 8 T_c dependence of the long spacing L' for A1 (●) and A2 (○) cast from the cyclohexane solution. The long spacings L for A1/PS1 (■) and A2/PS1 (□) with various compositions are also shown

DISCUSSION

In our previous studies on the crystallization of the crosslinked PCL-*b*-PB[29], the PCL block crystallized partially under the condition that the microdomain structure was completely fixed by the chemical crosslinks introduced in the system, though the crystallinity and crystallization rate were considerably reduced compared to the case of the un-crosslinked PCL-*b*-PB. We also observed the distortion of the microdomain structure by the subsequent crystallization, indicating that PCL-*b*-PB moved slightly in the fashion convenient to the crystallization. In the present case, however, the pure PCL-*b*-PS cannot move at all because one end (PS block) is anchored within the glassy region at T_c. This small difference in the mobility, though the molecule is extremely restricted in both cases, affects the crystallizability of the PCL block to lead the different morphologies in the systems.

The morphology formation in the crosslinked PCL-*b*-PB and PCL-*b*-PS is schematically illustrated in *Figure 9*, where a spherical microdomain structure with the PCL block inside is depicted and the plasticizer added to decrease T_g,*PS* is omitted for clarity. Of course, the plasticizer addition affects the microdomain structure considerably or it may bring the system into a wholly different structure

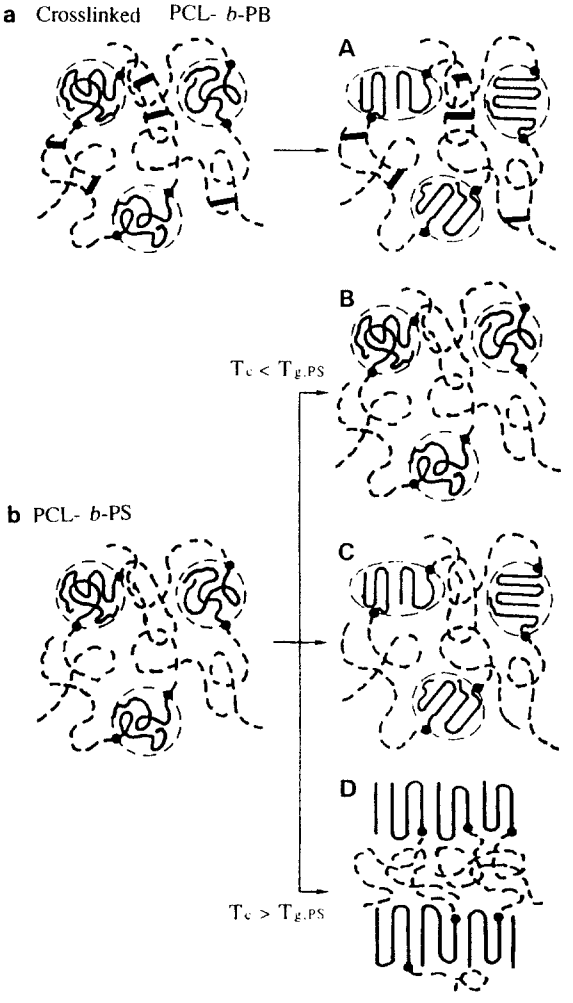

Figure 9 Schematic illustration showing the morphology formation in crosslinked PCL-*b*-PB (a) and PCL-*b*-PS (b). The spherical microdomain structure with the PCL block inside is depicted and the plasticizer added to decrease $T_{g,PS}$ in (b) is omitted for clarity. The thick line connecting the broken chains in (a) is the crosslinks introduced in the system

such as a homogeneous state at a small ϕ_{PS}. In the case of the crosslinked PCL-*b*-PB, the deformation of the existing microdomain structure makes the crystallization of the PCL block possible to yield the deformed microdomain structure in which the PCL block crystallizes partially (crystallized microdomain structure) (A in *Figure 9*). In the case of PCL-*b*-PS with $T_c < T_{g,PS}$, the microdomain structure of PCL-*b*-PS, though not observed in the present study, is rigid due to the glassy nature of the PS block to prevent completely the subsequent crystallization of the PCL block. As a result, the microdomain structure is preserved without any crystallization (B in *Figure 9*). When $T_{g,PS}$ decreases below T_c by adding the plasticizer, the molecular movement is possible and the PCL block crystallizes to result in the crystallized microdomain structure (C in *Figure 9*) or the lamellar morphology (D in *Figure 9*). The latter was observed in the relatively low molecular weight PCL-*b*-PB in our previous studies[8,11,15].

It is impossible to decide only from the SAXS results whether the final morphology is the crystallized microdomain structure or lamellar morphology, since we could not observe the microdomain structure at the melt by the SAXS measurement. If the spacing of the microdomain structure, D, is detectable, we can determine which morphology prevails in the system by comparing D with L; if $D \sim L$, the crystallized microdomain structure is formed and if D is extremely different from L, the morphological reorganization takes place to result in the lamellar morphology. Our previous study on the crystallization of the crosslinked PCL-*b*-PB[29], however, showed that T_m and χ decreased extremely due to the restricted crystallization of the PCL block within the existing microdomain structure. $T_{m,PCL}$ and χ shown in *Figure 2*b and *Figure 4*a are not small compared to those for the solution-cast PCL-*b*-PS (*Figure 7*a and b), where the lamellar morphology forms during the solvent evaporation. In addition, the SAXS curves shown in *Figure 5* have a clear second peak and the angular positions of first and second peaks definitely correspond to a ratio of 1/2, suggesting the lamellar morphology. The spacing shown in *Figure 6* is also extremely large when it is compared with the microdomain structure composed of amorphous–amorphous diblock copolymers (for example, $D = 19$ nm for the lamellar microdomain structure of styrene–2-vinylpyridine diblock copolymer with $M_{total} = 20\,000$[32] and $D = 17.2$ nm for the lamellar microdomain structure of styrene–isoprene diblock copolymer with $M_{total} = 21\,000$[33]). All the above results suggest that the lamellar morphology will be reasonably assumed for the morphology after crystallization of the PCL block in the plasticizer-added PCL-*b*-PS as well as the solution-cast PCL-*b*-PS.

The characteristics of the morphology, such as the long spacing and lamellar thickness, are dependent on the crystallization method employed as well as T_c, as observed in *Figures 6, and 8*. For the plasticizer-added PCL-*b*-PS, $T_{g,PS}$ is in close proximity to T_c even if the PCL block can crystallize. The PCL block is, therefore, somewhat restricted for the crystallization to lead the thinner lamellae with low χ. For the solution-cast PCL-*b*-PS, the PCL block can move freely during the solvent evaporation to form thicker lamellae with a high χ. The quantitative analysis is necessary for this point after confirming the resulting morphology by the crystallization of the PCL block.

CONCLUSIONS

In this study, various (PCL-*b*-PS) copolymers were synthesized, and the morphology and melting behaviour of PCL-*b*-PS were investigated by SAXS and d.s.c. measurements as a function of $T_{g,PS}$. A plasticizer miscible only with the PS block, such as PSO or DOP, was blended in order to decrease $T_{g,PS}$ successively. The following conclusions were obtained from the experimental results.

(1) The crystallinity of the PCL block, χ, was extremely influenced by $T_{g,PS}$, that is, the mobility of PCL-*b*-PS at T_c. When $T_c < T_{g,PS}$ the PCL block did not crystallize, while when $T_c > T_{g,PS}$ it crystallized partially to yield the morphology with a regular structure detectable by SAXS.
(2) The characteristics of the resulting morphology such as the long spacing and lamellar thickness were not determined by $T_{g,PS}$. It may be controlled by T_c rather than $T_{g,PS}$, as usually observed in crystalline homopolymers.
(3) The morphology formed in the plasticizer-added PCL-*b*-PS was qualitatively compared with that in the solution-cast PCL-*b*-PS. There was an appreciable difference in the long spacing, which will arise from the difference in the morphology formation between them. It is necessary for the further analysis to confirm the resulting morphology formed in the plasticizer-added PCL-*b*-PS.

ACKNOWLEDGEMENTS

This work was supported in part by Grants-in-Aid for Scientific Research (Nos. 08651072 and 09650992) from the Ministry of Education, Science, Sports, and Culture of Japan.

REFERENCES

1. Cohen, R. E., Cheng, P. L., Douzinas, K., Kofinas, P. and Berney, C. V., *Macromolecules*, 1990, **23**, 324.
2. Ishikawa, S., Ishizu, K. and Fukutomi, T., *Polymer Commun.*, 1991, **32**, 374.
3. Veith, C. A., Cohen, R. E. and Argon, A. S., *Polymer*, 1991, **32**, 1545.
4. Ishikawa, S., Sasaki, S. and Fukutomi, T., *J. Appl. Polym. Sci.*, 1993, **48**, 509.
5. Kofinas, P., Cohen, R. E. and Halasa, A. F., *Polymer*, 1994, **35**, 1229.
6. Khandpur, A. K., Macosko, C. W. and Bates, F. S., *J. Polym. Sci.*, 1995, **B33**, 247.
7. Unger, R., Beyer, D. and Donth, E., *Polymer*, 1991, **32**, 3305.
8. Nojima, S., Kato, K., Yamamoto, S. and Ashida, T., *Macromolecules*, 1992, **25**, 2237.
9. Rangarajan, P., Register, R. A. and Fetters, L. J., *Macromolecules*, 1993, **26**, 4640.
10. Lovinger, A. J., Han, B. J., Padden, F. J. and Mirau, P. A., *J. Polym. Sci.*, 1993, **B31**, 115.
11. Nojima, S., Nakano, H., Takahashi, Y. and Ashida, T., *Polymer*, 1994, **35**, 3479.
12. Rangarajan, P., Register, R. A., Adamson, D. H., Fetters, L. J., Bras, W., Naylor, S. and Ryan, A. J., *Macromolecules*, 1995, **28**, 1422.
13. Ryan, A. J., Hamley, I. W., Bras, W. and Bates, F. S., *Macromolecules*, 1995, **28**, 3860.
14. Rangarajan, P., Register, R. A., Fetters, L. J., Bras, W., Naylor, S. and Ryan, A. J., *Macromolecules*, 1995, **28**, 4932.
15. Nojima, S., Yamamoto, S. and Ashida, T., *Polym. J.*, 1995, **27**, 673.
16. Yang, Y. W., Tanodekaew, S., Mai, S. M., Booth, C., Ryan, A. J., Bras, W. and Viras, K., *Macromolecules*, 1995, **28**, 6029.
17. Gervais, M. and Gallot, B., *Makromol. Chem.*, 1977, **178**, 1577.
18. Gervais, M. and Gallot, B., *Polymer*, 1981, **22**, 1129.
19. Gervais, M., Gallot, B., Jerome, R. and Teyssie, P., *Makromol. Chem.*, 1981, **182**, 989.
20. Gast, A. P., Vinson, P. K. and Cogan-Farinas, K. A., *Macromolecules*, 1993, **26**, 1774.

21. Liu, L., Jiang, B. and Zhou, E., *Polymer*, 1996, **37**, 3937.
22. Liu, L., Yeh, F. and Chu, B., *Macromolecules*, 1996, **29**, 5336.
23. Ito, K. and Yamashita, Y., *Macromolecules*, 1978, **11**, 68.
24. Richardson, M. J. and Savil, N. G., *Polymer*, 1977, **18**, 3.
25. Crescenzi, V., Manzini, G., Galzolari, G. and Borri, C., *Eur. Polym. J.*, 1972, **8**, 449.
26. Chatani, Y., Okita, Y. and Tadokoro, H., *Polym. J.*, 1970, **1**, 555.
27. Nojima, S., Terashima, Y. and Ashida, T., *Polymer*, 1986, **27**, 1007.
28. Nojima, S., Satoh, K. and Ashida, T., *Macromolecules*, 1991, **24**, 942.
29. Nojima, S., Hashizume, K., Rohadi, A. and Sasaki, S., *Polymer*, 1997, **38**, 2711.
30. Nojima, S., Kuroda, M. and Sasaki, S., *Polym. J.*, 1997, **29**, 642.
31. Wunderlich, B., *Macromolecular Physics 3*, Academic Press, New York, 1980.
32. Matsushita, Y., Mori, K., Mogi, Y., Saguchi, R., Noda, I., Nagasawa, M., Chang, T., Glinka, C. J. and Han, C. C., *Macromolecules*, 1990, **23**, 4317.
33. Hashimoto, T., Shibayama, M. and Kawai, H., *Macromolecules*, 1980, **13**, 1237.